Applied Catalysis B: Environmental 127 (2012) 307–315

Contents lists available at SciVerse ScienceDirect

Applied Catalysis B: Environmental

journal homepage: www.elsevier.com/locate/apcatb

Effect of precursor on the performance of alumina for the dehydration of methanol to dimethyl ether

Ahmed I. Osman[a,b], Jehad K. Abu-Dahrieh[a], David W. Rooney[a,*], Samih A. Halawy[b], Mohamed A. Mohamed[b], Adel Abdelkader[b]

[a] CenTACat, Queen's University Belfast, Belfast BT9 5AG, Northern Ireland, UK
[b] Chemistry Department, Faculty of Science - Qena, South Valley University, Qena 83523, Egypt

ARTICLE INFO

Article history:
Received 21 June 2012
Received in revised form 7 August 2012
Accepted 28 August 2012
Available online 6 September 2012

Keywords:
DME
Methanol dehydration
Acid catalyst
η-Al_2O_3
γ-Al_2O_3

ABSTRACT

Dimethyl ether (DME) is amongst one of the most promising alternative, renewable and clean fuels being considered as a future energy carrier. In this study, the comparative catalytic performance of γ-Al_2O_3 prepared from two common precursors (aluminum nitrate (AN) and aluminum chloride (AC)) is presented. The impact of calcination temperature was evaluated in order to optimize both the precursor and pre-treatment conditions for the production of DME from methanol in a fixed bed reactor. The catalysts were characterized by TGA, XRD, BET and TPD-pyridine. Under reaction conditions where the temperature ranged from 180 °C to 300 °C with a WHSV = 12.1 h^{-1} it was found that all the catalysts prepared from AN(η-Al_2O_3) showed higher activity, at all calcination temperatures, than those prepared from AC(γ-Al_2O_3). In this study the optimum catalyst was produced from AN and calcined at 550 °C. This catalyst showed a high degree of stability and had double the activity of the commercial γ-Al_2O_3 or 87% of the activity of commercial ZSM-5(80) at 250 °C.

1. Introduction

A growing awareness of climate change, air pollution and energy consumption necessitates the development of clean, renewable and sustainable fuels. In terms of small energy generators for either fixed or mobile power sources there are a number of existing technologies, of which diesel engines are common. However, unless legislated against, such engines produce exhaust streams with significant amounts of NO_x, SO_x and particulates. Furthermore diesel exhausts have been linked to cancer [1] in a recent World Health Organization report, thus clean alternatives are again desired [2]. Dimethyl ether (DME) is one of the most promising ultra clean, renewable and oxygenated alternative fuel for diesel engines. The reasons for this are numerous and include its lower auto-ignition temperature (cetane number, CN > 55), higher oxygen content (34.8% by mass) and C—O—C molecular structure. DME can be easily evaporated [3] is non-toxic, non-carcinogenic and non-corrosive. It is also considered as an environmentally friendly compound because of its low global warming potential over both short and long time horizons [4].

There are two main ways to produce DME, either by methanol dehydration over a solid acid catalyst or direct synthesis from synthesis gas over hybrid catalysts comprising metal oxide (i.e. methanol synthesis) and a solid acid (i.e. methanol dehydration). Both of these reactions are shown below [5].

$$3CO + 3H_2 \leftrightarrow CH_3OCH_3 + CO_2 \quad (1)$$

$$2CH_3OH \leftrightarrow CH_3OCH_3 + H_2O \quad (2)$$

Methanol to DME (MTD) dehydration over a solid acid catalyst in a fixed bed reactor was first reported by Mobil in 1965. Since then, many methanol dehydration catalysts have been examined [5] including γ-Al_2O_3 [2,6–9], crystalline aluminosilicates [9,10], zeolites (ZSM-5) [11], clays [12] and phosphates such as aluminum phosphate [13,14]. However the most common catalysts used are γ-Al_2O_3 and zeolites.

The activity of H-type zeolites has been reported for the dehydration of methanol to DME [15–19]. These zeolites are characterized by their high acidity, however, such high acidity can result in significant coke formation and consequently fast deactivation [20]. Furthermore methanol can undergo secondary reactions to produce hydrocarbons at temperatures higher than 240 °C [16]. Coke deposition on the surface of catalysts has been observed in the case of strong acid catalysts [2,21,22], and thus formation of coke as side product was reported as a disadvantage of using zeolites in MTD reaction. However, γ-Al_2O_3 has a low activity at temperatures lower than 300 °C were no hydrocarbons are formed thus

* Corresponding author at: School of Chemistry and Chemical Engineering, Queen's University Belfast, David Keir Building, Stranmillis Road, Belfast BT9 5AG, Northern Ireland, UK. Tel.: +44 2890 97 4050; fax: +44 2890 97 4687.
E-mail address: d.rooney@qub.ac.uk (D.W. Rooney).

0926-3373/$ – see front matter © 2012 Published by Elsevier B.V.
http://dx.doi.org/10.1016/j.apcatb.2012.08.033

giving a total selectivity for DME of 100%[16]. Also γ-Al_2O_3 is associated with weak to medium acidic sites, and thus is preferable in the MTD reaction [14] providing greater coke stability and lower by-product formation [8].

Alumina is one of the most important structural materials with several transition phases that have enormous technological and industrial significance [23]. It is thus the most common catalyst and catalyst support used in heterogeneous catalysis due to its low cost, good thermal stability, high specific surface area, surface acidity and interaction with deposited transitional metals [24]. The γ-phase in particular is one of the polymorphic phases of alumina with numerous applications [23]. Alumina exists in eight different polymorphs – seven metastable phases (γ, κ, ρ, η, θ and χ) as well as the thermally stable α-phase. The metastable (also known as transition) phases of alumina are intrinsically nanocrystalline in nature and can be easily synthesized by a variety of methods. γ-Al_2O_3 can be transformed into a different phase under heat treatment with this transformation sequence being illustrated as follows: [25]

$$\gamma - Al_2O_3 \xrightarrow{750^\circ C} \delta \xrightarrow{900^\circ C} \theta \xrightarrow{1200^\circ C} \alpha \quad (3)$$

Boehmite, aluminum oxyhydroxide (AlO(OH)), is a versatile material employed in domains such as sol–gel ceramics, surface coatings, rheology control, and pharmaceuticals [26]. It is also an important precursor in preparing alumina. γ-Al_2O_3, is commonly produced from boehmite by calcination at 500 °C in air [26], and those modified with silica, phosphorus or B_2O_3 are current commercial catalysts for the dehydration of methanol to DME [26].

Seo et al. [27] studied the influence of structure type of Al_2O_3 on the dehydration of methanol to dimethyl ether. Catalysts (γ-Al_2O_3 and η-Al_2O_3) were prepared from boehmite and bayerite, respectively, via calcination at various temperatures and the effect of alumina properties on the catalytic performance evaluated. In their study it was noted that with heat treatment, the properties of alumina changed significantly. For example it was identified that the particle size of γ-Al_2O_3 increased with increasing calcination temperature while the total amount of acidic sites over γ-Al_2O_3 decreased. It was reported that the total acidity of alumina calcined at 400 °C (which was shown by XRD to be composed of γ-Al_2O_3 + boehmite phases) was 80.6 ± 2.2 μmol/g while γ-Al_2O_3 calcined at 500 °C was 67.7 ± 0.00 μmol-NH_3/g-catalyst.

Transition aluminas are widely used as catalysts and catalyst supports in many industrial processes, in particular those related to petroleum refining [28]. Knozinger and Ratnasamy [28] studied the nature of aluminas and they proposed models for it. They reported that the nature of the surface hydroxyl on γ-Al_2O_3 depend on the surface microstructure and therefore differed on each crystal plane.

Clearly the preparation method affects the activity of the catalysts as activity varies with both precursor type and the preparation procedure. For alumina there are a number of different preparation methods which can be used. For example γ-Al_2O_3 can be prepared from different precursors as aluminum nitrate [2,29], aluminum chloride [23,30] or from aluminum isopropoxide [6,8,26]. In this work a comparative study was performed between the two cheapest and most readily available precursors which are aluminum nitrate and aluminum chloride. This was in order to identify which one was the best at producing an active catalyst with latter tests conducted to benchmark them against commercial materials. The effect of calcination temperature was also studied to find a catalyst with the highest catalytic performance for methanol dehydration to DME. Long term stability tests were also performed for the best active catalysts identified and again these were benchmarked against commercial materials.

2. Experimental

2.1. Materials and methods

The chemicals used in the present study were all analytical grade and supplied by Aldrich, UK. These included aluminum nitrate nonahydrate [$Al(NO_3)_3{\cdot}9H_2O$], ammonia solution (35%) and aluminum chloride anhydride ($AlCl_3$).

2.2. Catalyst preparation

Catalysts were prepared from two precursors namely $Al(NO_3)_3{\cdot}9H_2O$ and $AlCl_3$ $Al(NO_3)_3{\cdot}9H_2O$ was first dissolved in deionized water with continuous stirring at 60 °C. When the solution was completely mixed and heated to 100 °C, ammonia solution was added dropwise. After the addition of the ammonia solution was completed stirring continued for a further 12 h at room temperature (approx. 18 °C). The pale off-white precipitate was filtered, washed, and dried at 120 °C overnight. The precipitate was then calcined at either 300 or 550 °C for 4 h. The catalysts that dried at 120 °C and those calcined at 300, 550 °C are designated as AN120, AN300 and AN550, respectively.

The same procedure was followed for the catalysts prepared from the $AlCl_3$ precursor. In this case and after filtration of the precipitate, the powders were thoroughly washed with hot water to remove any soluble chloride. The removal of chlorine was verified by a $AgNO_3$ test. Here a sample of the filtrate was taken and a drop silver nitrate added, if this formed a precipitate or turbid solution would indicate the presence of chorine in the sample. In this case detectable levels of chlorine were not found. After drying at 120 °C overnight, the precipitate was calcined at 300, 370, 550, 650 and 750 °C, respectively. As above the catalysts that were dried at 120 and calcined at 300, 370, 550, 650 and 750 °C are designated as AC120, AC300, AC370, AC550, AC650 and AC750, respectively. All the catalysts (dried and calcined) were further tested for chlorine content using Oxygen Flask analysis discussed below.

The commercial γ-Al_2O_3 (BET = 117 m^2/g) was prepared by crushing γ-Al_2O_3 pellets (Alfa Aesar). Commercial NH_4-ZSM-5 zeolite (Alfa Aesar) with (SiO_2/Al_2O_3 = 80) (BET = 425 m^2/g) was also used, for simplicity this catalyst is designated and labeled as HZSM-5(80).

2.3. Catalyst characterization

Thermogravimetry (TGA) was performed from ambient to 600 °C at a heating rate of 10 °C/min, in a stream of dry N_2 flowing at 40 cm^3 min^{-1}, using a Perkin-Elmer Thermogravimetric analyzer Pyris 1TGA. Changes in mass of the sample were recorded during the ramping operation.

Powder X-ray diffraction (XRD) experiments of the catalysts were carried out using a PANalytical X'Pert Pro X-ray diffractometer. This diffractometer is equipped with a CuKα X-ray source with wavelength of 1.5405 Å. The diffractograms were collected from 10° to 89°. The X-ray detector was set at 40 kV and 40 mA. Once the scan had finished, the main peaks were selected and compared to diffraction patterns in the software library. The pattern with the highest percentage match was used.

Brunauer–Emmett–Teller (BET) analysis was performed using using a Micromeritics ASAP 2010 system. The BET surface areas and pore volumes were measured by N_2 adsorption and the desorption isotherm at liquid nitrogen temperature (−196 °C).

The chlorine content was measured using Oxygen Flask analysis by combusting the sample in an oxygenated flask containing water, then shaking; in which chlorine dissolved in water forming HCl, the later was titrated with 0.02 M Hg_2NO_3 to find % Cl.

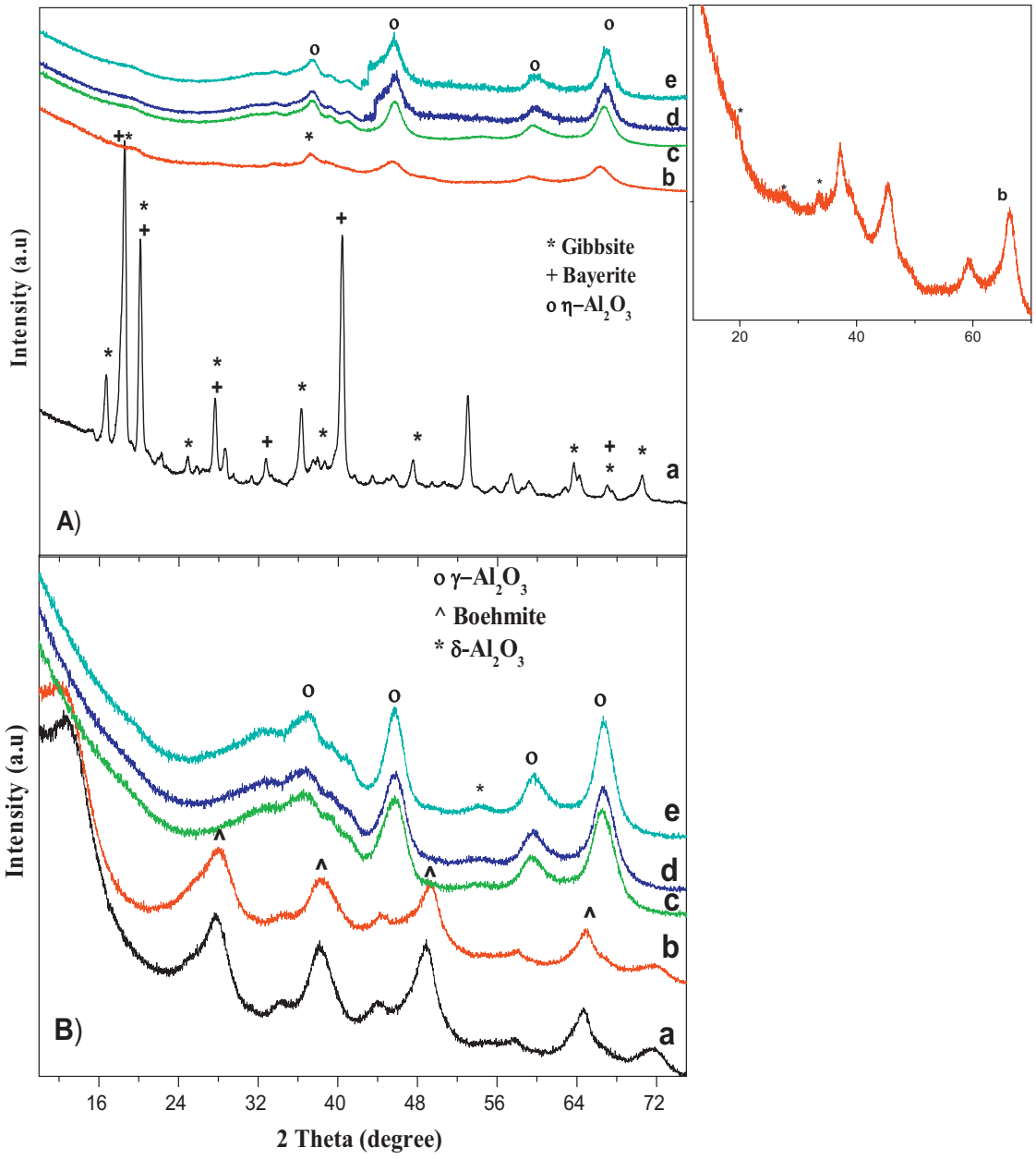

Fig. 1. (A) XRD patterns of different acid catalysts prepared from aluminum nitrate precursor, (a) AN120, (b) AN300, (c) AN550, (d) AN650 and (e) AN750; (B) XRD patterns of different acid catalysts prepared from aluminum chloride precursor, (a) AC120, (b) AC300, (c) AC550, (d) AC650 and (e) AC750.

Table 1
Properties of the catalysts.

Catalyst abbreviation	Chlorine (%)	Surface area		Particle size (nm)	Total acidity[a], A (sites/g)	Acid site density[b], B (sites/m^2)	DME yield (%)[c]
		S_{BET} (m^2/g)	Pore volume (cm^3/g)				
AN120	Nil	369	0.15	18.1	–	–	44.4
AN300	Nil	300	0.2	4.3	18.75	6.3	72.7
AN550	Nil	223	0.5	5.5	8.56	3.8	86.9
AN650	Nil	189	0.41	6.4	7.02	3.7	88
AN750	Nil	169	0.31	8	4.83	2.9	64.1
AC120	1.2	378	0.20	3.1	–	–	10.7
AC300	0.8	308	0.22	3.1	11.05	3.5	14.2
AC550	0.38	278	0.35	3.7	6.91	2.5	43
AC650	0.2	230	0.31	3.8	5.52	2.4	60.3
AC750	0.15	187	0.30	4.4	4.20	2.24	40.4
γ-Al_2O_3	Nil	117	0.42	5.9	4.11	3.51	40
HZSM-5(80)	Nil	425	0.17	2.9	9.82	2.31	89

[a] Total acidity = A × 10^{20}.
[b] Acid site density = B × 10^{18}.
[c] T = 250 °C; He flow rate = 80 ml/min; WHSV: 12.1 h^{-1}.

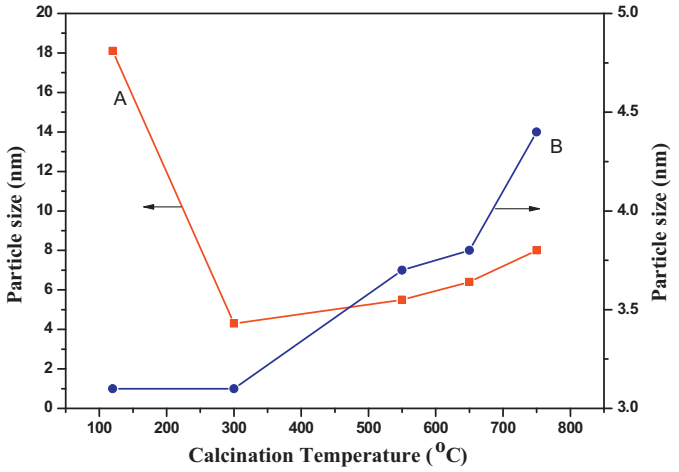

Fig. 2. The effect of calcination on particle size for AN samples (A) and AC samples (B).

The total number of acidic sites (sites m^{-2}) over each catalyst were measured using the temperature programmed desorption of pyridine (TPD-pyridine) as the probe molecule. The details have been described previously [31,32]. This was performed using 50 mg of the catalyst after pretreatment at 250 °C for 2 h in air before the exposure to the probe molecule. 15–20 mg of pyridine–covered samples were subjected to TG analysis on heating up to 600 °C (at 20 °C/min heating rate) in dry N_2 (flow rate = 40 ml/min). The mass loss due to desorption of pyridine from the acidic sites, was determined as a function of total surface acidity as sites $g^{-1}{}_{cat}$. The equation used to calculate the acid density site as follows:

$$\text{Acid site density} = \frac{\text{moles of pyridine desorped} \times \text{Avogdro's number (sites/mol)}}{\text{wt. of catalyst sample (g)} \times \text{BET (m}^2\text{/g)}} \quad (4)$$

The determination of Lewis/Brönsted acid sites in the synthesized catalysts was performed by diffuse reflectance infrared fourier transform (DRIFT) experiments of adsorbed pyridine using a Bruker Vertex 70 FTIR Spectrometer equipped with a liquid N_2-cooled detector instrument. Samples were pre-treatment before measuring. This was achieved by outgassing at 120 °C for 0.5 h under an Ar atmosphere. Subsequently the samples were saturated with pyridine at 50 °C then the pysisorbed pyridine was removed by flushing with Ar gas for 0.5 h. Fresh samples were used to record the IR background under Ar flow at 300 °C. Then, the pyridine (Py) adsorbed samples were placed in the DRIFT cell at 40 °C. The samples were heated under Ar at the flow rate of 50 cm^3 min^{-1} and the in situ DRIFT spectra were measured with a resolution of 4 cm^{-1} and with an accumulation of 56 scans every 30 s. The resulted spectra after pyridine desorption were substracted from those measured before pyridine adsorption (fresh samples) in order to determine the bands relative to Lewis and Brönsted acidic sites.

Further characterization of the catalysts by scanning electron microscopy (SEM) was performed using a JEOL JSM-6500F (Field Emission Scanning Microscope) operated at 5 kV.

2.4. Catalyst activity

The activity testing was carried out in an isothermal fixed-bed reactor made of stainless steel (6 mm OD). The catalyst bed consisted of 100 or 200 mg (250–425 μm) of catalyst placed in between two plugs of quartz wool. Aera mass flow controllers were used to control the flow of He to the reactor. The liquid methanol was injected by patented Cheminert® M Series liquid handling pump. A stable flow of methanol vapor to the reactor was established by passing the combined flow He and methanol through a saturator system. The evaporation chamber was kept at 150 °C. In order to prevent any condensation, all of the lines were heated to 150 °C. This mixture was then fed to the fixed bed reactor. The reaction conditions used 20% methanol under atmospheric pressure and over a temperature range from 180 °C to 300 °C. The total flow rate was 100 cm^3 min^{-1}. Before the reaction, the catalyst was activated in a stream of pure He at 325 °C for 0.5 h under atmospheric pressure. Then, the methanol and He mixture was fed to the reactor and samples analyzed by gas chromatography (Perkin-Elmer 500) equipped with a thermal conductivity detector (TCD) and a flame ionization detector (FID). A Hayesep DB column was used for the separation of CO, CO_2, DME, MeOH, CH_4, C_2H_4, C_2H_6, ethanol, propanol, and butanol.

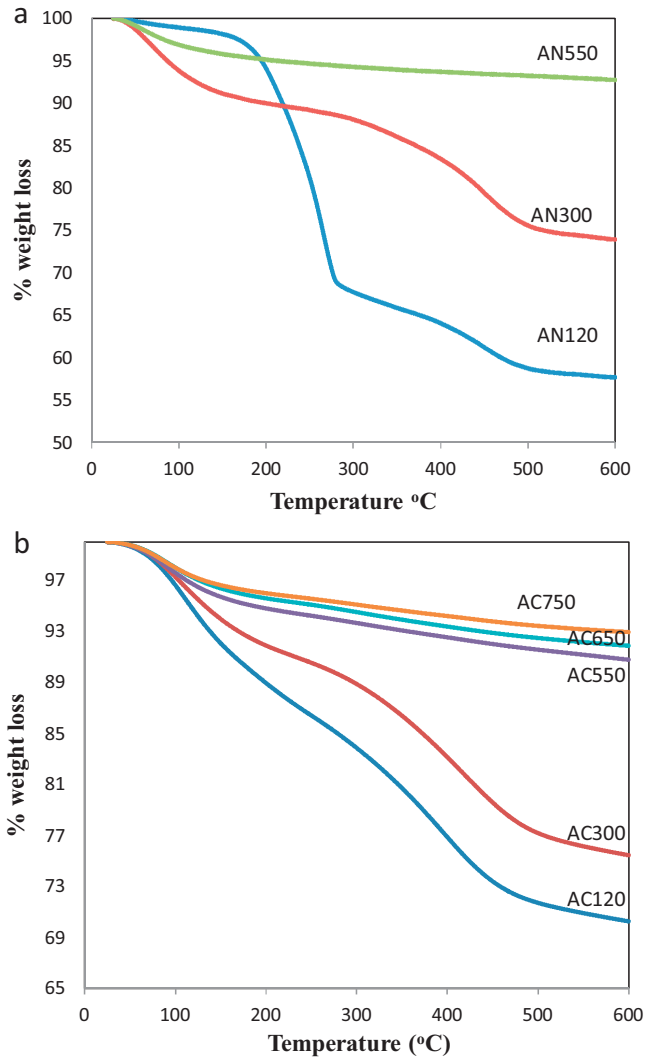

Fig. 3. TGA curves for the catalysts in N_2 atmosphere with heating rate 10 °C/min.

The methanol conversion (X_{MeOH}) (Eq. (5)) was calculated based on the molar flow rate of methanol in the feed ($F_{MeOH,in}$) and in the outlet stream ($F_{MeOH,out}$):

$$X_{MeOH} = \frac{F_{MeOH,in} - F_{MeOH,out}}{F_{MeOH,in}} \quad (5)$$

DME yield (Y_{DME}) was determined in Eq. (6) as the ratio (expressed in molar flow rate) between the actual moles of the product DME that are present in the reactor outlet stream and theoretical moles of the product DME:

$$Y_{DME} = \frac{F_{DME,actual}}{F_{DME,theoretical}} \times 100\% \quad (6)$$

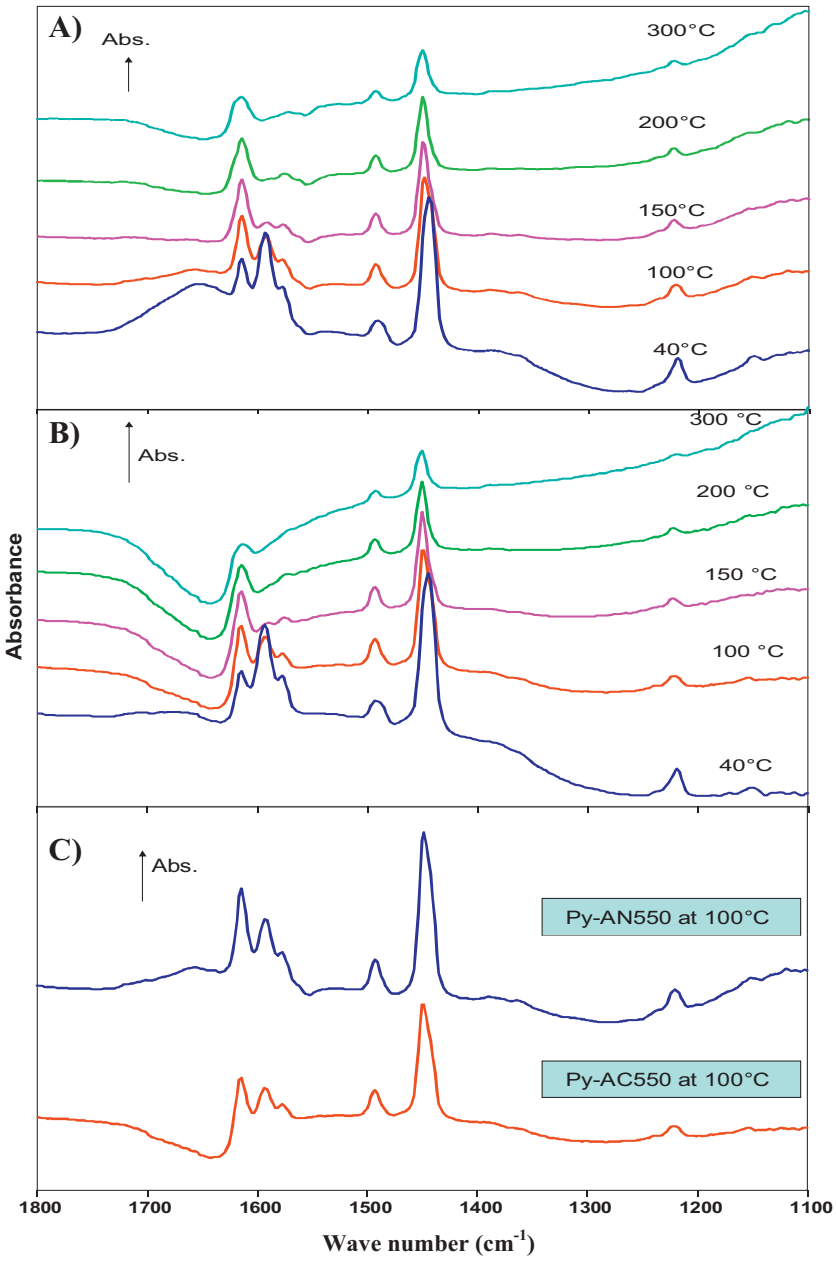

Fig. 4. In situ DRIFTS spectra of pyridine desorption pyridine adsorbed on AC550 (A), AN550 (B) following thermal treatment and the comparison between pyridine-AN550 and pyridine-AC550 at 100 °C (C) in the region 1800–1100 cm^{-1}.

DME formation rate (r_{DME}) was determined in Eq. (7) as the actual moles of the product DME that are present in the reactor outlet stream per gram catalyst:

$$r_{DME} = \frac{F_{DME,actual}}{\text{wt. of the catalyst}} \times 100\% \quad (7)$$

3. Results and discussion

3.1. Catalyst characterization

3.1.1. X-ray diffraction (XRD) analysis

Fig. 1A displays the XRD patterns of AN120, AN300, AN550, AN650 and AN750 (a, b, c, d and e, respectively). Diffractogram (a) showed a mixture of Bayerite (JCPDS 20-11) and Gibbsite (JCPDS 33-18) in which Bayerite is the most prominent peak. As Bayerite has the highest symmetry among all $Al(OH)_3$ structures it is the most thermodynamically stable phase, and thus the initially formed crystalline phase [33,34]. Bayerite is formed at room temperature and transforms to Gibbsite with high crystallinity. The high and sharp diffraction peak in diffractogram (a) indicates that the obtained mixture phases have a large crystalline size (see Table 1) [32]. Diffractogram (b) showed mixture of diffraction lines that correspond to undecomposed gibbsite (JCDD 33-18) and η-Al_2O_3 (JCDD 04-0875). On further increasing the temperature to 500 °C, it will convert to η-Al_2O_3, and therefore diffractogram c, d and e showed only diffraction lines belonging to η-Al_2O_3 (JCDD 04-0875).

Fig. 1B displays the XRD patterns of AC120, AC300, AC550, AC650 and AC750 (a), (b), (c), (d), (e) and (f), respectively). Diffractograms a and b showed the diffraction lines that correspond to γ-AlO(OH) (JCDD 21-1307), while diffractogram c and d showed the diffractogram of γ-Al_2O_3 (JCDD 10-0425). Diffractogram e showed the

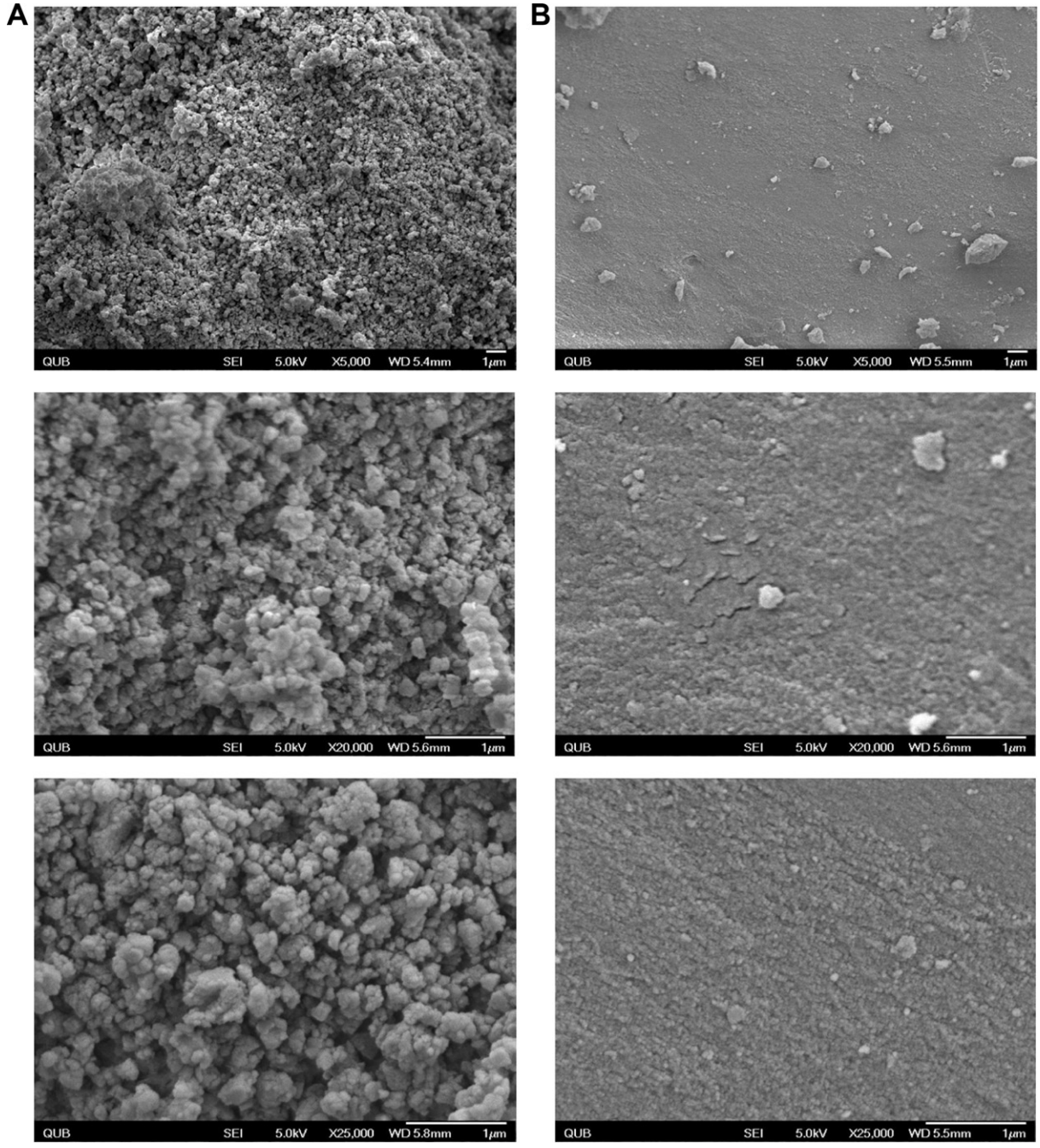

Fig. 5. Representative SEM micrographs of (A) AN550 and (B) AC550 with magnification 5000, 20,000 and 25,000, respectively.

two diffraction lines that correspond to γ-Al_2O_3 (JCDD 10-0425) and δ-Al_2O_3 (JCPDS 16-0394) [25,35], the appearance of the new δ-Al_2O_3 is known to affect the catalytic performance of the catalyst during the MTD reaction as will be discussed later. It is apparent from this data that the bulk structures of γ- and η-Al_2O_3 are very similar to each other, and in some instances are considered to be identical [33,36,37].

For all catalysts, the particle size of γ-Al_2O_3 increased with increasing calcination temperature which is in agreement with Seo et al. [27]. The large particle size for the AN120, i.e. the dried catalyst, is attributed to the mixture of gibbsite and bayerite as mentioned above (see Table 1 and Fig. 2). This then initially decreases with calcination at 300 °C and thereafter increases as in the case of the chloride precursor.

3.1.2. TGA

All the catalysts were subjected to TGA analysis to show the suitable temperature of calcinations AC and AN catalysts for obtaining γ-Al_2O_3 and η-Al_2O_3 phase, respectively. As seen in Fig. 3A, for AN120 catalyst, three weight loss steps corresponding to the phase transformations to η-Al_2O_3 are observed. The first step started at 50 °C followed by two consecutive steps in the range 120–270 °C and 270–500 °C. After that, the rate of weight loss during heating up to 600 °C slowed with the formation of η-Al_2O_3. The total weight loss % calculated from ambient up to 600 °C is equal to 42.3%. Theoretically, the transformation of Gibbsite $Al(OH)_3$ to η-Al_2O_3 should be associated with 34.6% weight loss. The difference in weight loss of 7.68% can be attributed to the desorption of physisorbed water [38]. For the AN300 catalyst, the percentage weight loss was 24.5%.

This is due to the AN300 having already undergone partial conversion from undecomposed gibbsite phase to the η-Al_2O_3) phase. Here again the difference in weight loss 9.3% can be also attributed to the desorption of physisorbed water [38] as well as dehydroxylation occurring when gibbsite transformed into η-Al_2O_3 [30]. For AN550 catalyst, the weight loss is 7.3% which can be attributed to the desorption of physisorbed water [38], as there is no weight loss due to the complete transformation to η-Al_2O_3. From Fig. 3A, the most suitable temperature to prepare η-Al_2O_3 is 550 °C and is in good agreement with the XRD data.

Fig. 3B presents the TGA for the catalysts prepared from aluminum chloride precursor (AC120, AC300, AC370, AC550, AC650 and AC750). Here the weight loss was 29.6, 26.3, 7.7, 7.3 and 6.3, respectively. As above the XRD showed that Boehmite was formed at 120 °C. Thus the theoretical transformation from boehmite to γ-Al_2O_3 should be associated with 15% weight loss, again the differences are attributed here to the desorption of physisorbed water and possible any traces of chlorine remaining in the bulk of AC catalysts (see Table 1).

Fig. 4 shows the infrared spectra of the pyridine adsorbed on AC550 (A), AN550 (B) following thermal treatment and the comparison between Py-AN550 and Py-AC550 at 100 °C (C) in the region 1800–1100 cm^{-1}. Spectrum (A) exhibited absorbance bands at 1222, 1445, 1488, 1577, 1596, 1618 and 1653 cm^{-1}. Bands observed at 1445 and 1596 cm^{-1} in the spectra are attributed to the presence of hydrogen bonded pyridine adsorbed on Lewis acid sites [39,40]. Strong Lewis bound pyridine (at 1623 and 1455 cm^{-1}) and weak Lewis bound pyridine at 1575 cm^{-1} [40]. The band observed at about 1488 cm^{-1} is due to adsorbed pyridine on both Lewis and Brönsted acid sites. The band at 1653 cm^{-1} relates to stretching and bending modes of adsorbed water [38]. The band at 1222 cm^{-1} is due to Al–O–Al symmetric and asymmetric bending modes [38]. From diffractogram (A), AN550 showed bands relative to Lewis acidic with strong sites at 1623 and about 1455 cm^{-1}, a small band related to weak lewis acid sites (1575) and another small band related to Lewis and Brönsted (1488 cm^{-1}) sites. It is clear from DRIFTs spectra that the Lewis acidic sites are responsible for the acidity in AN550 (η-Al_2O_3) and AC550 (γ-Al_2O_3) which is in agreement with Seo et al. results [27].

Spectrum (B) exhibited the same features to that of AN550, except that the intensity of the absorption bands in AC550 are lower than that of AN550, which is clear in spectrum (C). DRIFT spectra (C) give clear evidence that AN550 is higher acidity than AC550.

Fig. 5 shows the SEM images of AN550 and AC550. As seen from these there is a difference in the morphology of the particles. Clearly the AC550 produces a much smoother surface. It can thus be concluded from the SEM that the surface roughness is very different between the AN550 and AC550 catalysts.

3.2. Catalyst activity

Fig. 6 shows the effect of calcination temperature of AN and AC catalysts for reactions carried out over the temperature range 180–300 °C. It is clear from Fig. 6A that for each reaction temperature, above a minimum of approximately 200 °C, that the methanol conversion increased until a maximum at calcination temperature of 650 °C, after which it decreases sharply. The particle size of γ-Al_2O_3 increased as the calcination temperature increased. In the temperature range from 300 °C to 650 °C, the particle size of the samples was comparable (see Table 1). As the temperature increased to 750 °C, the change was significant (15.8%). This change was accompanied with a decrease in acid site density of 6.7% and the presence of new δ-Al_2O_3 phase[25] with the γ-Al_2O_3 (see Fig. 1B graph e), it may cause a sharp decrease in catalytic activity of AN750 as shown in Fig. 4A. Therefore as expected the properties of the acid sites and their density within the alumina change with the

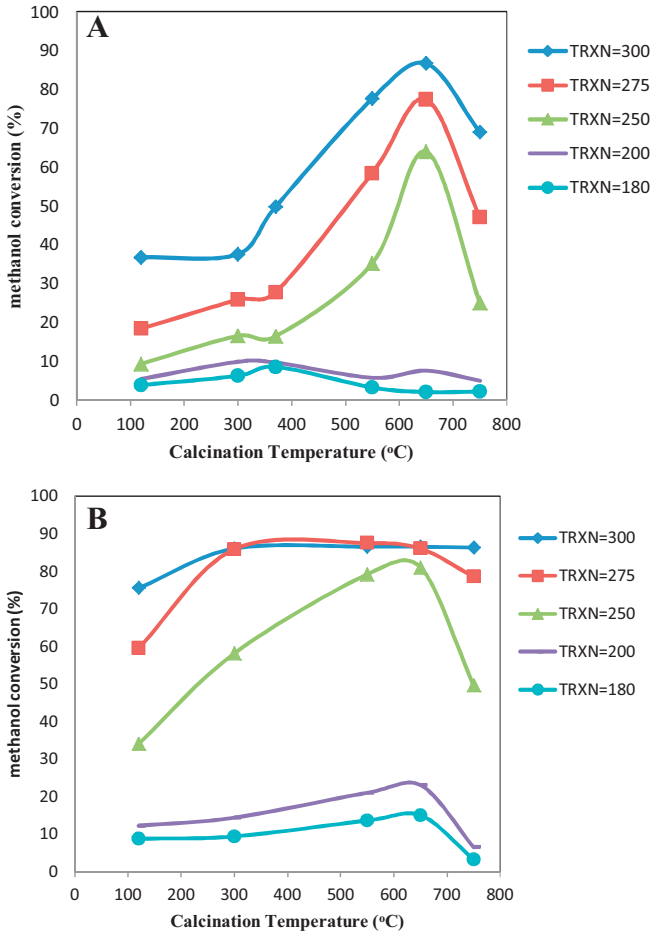

Fig. 6. Effect of calcination temperature on methanol conversion over catalysts; (A): prepared from AC precursor; (B): prepared from AN precursor; at different reaction temperature. (T = 180–300 °C; catalyst weight = 200 mg; He flow rate = 80 ml/min; WHSV: 12.1 h^{-1}).

calcination temperature (see Table 1). It can be seen from Fig. 6B that for each reaction temperature the methanol conversion increased until a maximum was found between 550 °C and 650 °C. This maximum is less clearly defined than in the case of the AC catalysts. The decrease of activity at calcination temperature of 750 °C may be attributed to the structure of η-Al_2O_3 calcined at 750 °C which partially collapsed resulting in a decrease in acid site density [27] and an associated decrease in catalytic activity.

Fig. 7 shows the effect of temperature on the activity of solid acid catalysts prepared using different aluminum precursors. But as shown in Fig. 7A, as the temperature increased the activity increased for all catalysts in the following sequence: AN650 > AN550 > AN300 > AN750 > AN120. Clearly the thermodynamic equilibrium conversion for AN300, AN550 and AN650 is obtained at temperatures greater than 275 °C. Given the equilibrium constraints the conversion of methanol does not exceed 86.5% and thus the maximum conversion of methanol is limited under the reaction conditions (300 °C) employed. It can be seen from Fig. 7B that all catalysts exhibited low activity at reaction temperatures below 200 °C regardless the calcinations temperature, and is attributed to the low activity of alumina at such temperatures. Fu et al. [16] and Jiang et al. [11] studied the effect of temperature on the activity of γ-Al_2O_3 for dehydration of methanol to DME. They found that γ-Al_2O_3 exhibited low activity at temperatures below 300 °C. As the reaction temperature increased, the methanol conversion increased for all catalysts in the following sequence: AC650 > AC550 > AC750 > AC300 > AC120. However it is clear from

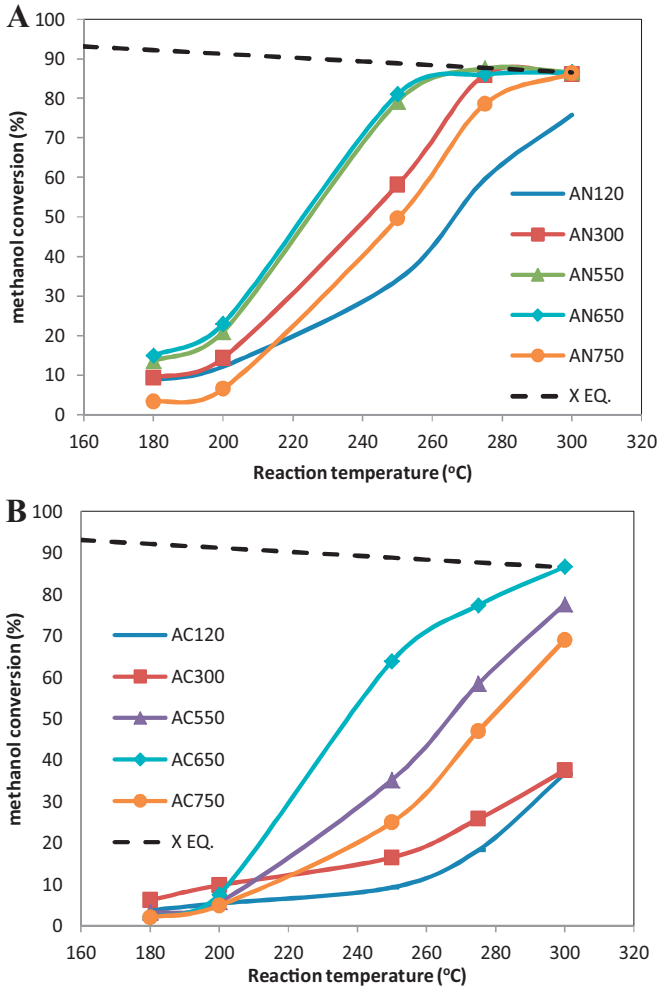

Fig. 7. Effect of reaction temperature on methanol dehydration to DME over catalysts prepared using different precursor at different calcination temperature. (A) Aluminum nitrate and (B) aluminum chloride. (T = 180–300 °C; catalyst weight = 200 mg; He flow rate = 80 ml/min; WHSV: 12.1 h^{-1}).

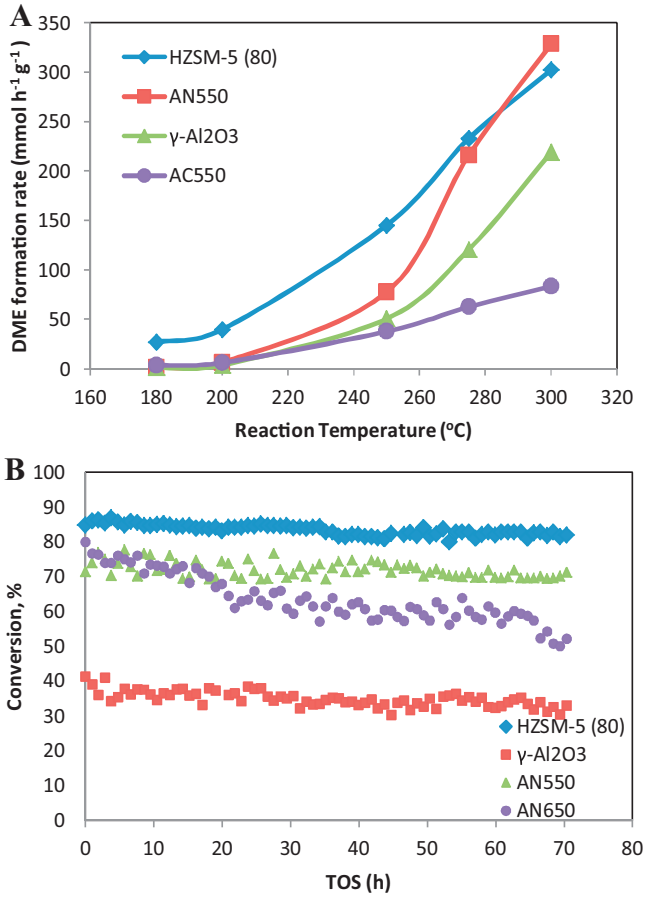

Fig. 8. (A) Effect of reaction temperature on DME formation rate over catalysts (AN550, commercial γ-Al_2O_3 and commercial HZSM-5(80)); (B) MeOH conversion with time on stream over HZSM-5(80), commercial γ-Al_2O_3, AN550 and AN650. (T = 250 °C; catalyst weight = 200 mg; He flow rate = 80 ml/min; WHSV: 12.1 h^{-1}).

Fig. 7A and B that the most active catalysts at all reaction temperatures are AN550 and AN650 from aluminum nitrate precursor and AC650 from aluminum chloride precursor.

As shown in Fig. 7, AN catalysts are higher in activity than AC catalysts at the same calcination temperature. For instance, AN550 (η-Al_2O_3) and AC550 (γ-Al_2O_3) were calcined at 550 °C however there are significant differences in methanol conversion especially at reaction temperatures higher than 200 °C. Such differences could be attributed to differences in surface area, total acid sites, acid density, morphology and structure. From Table 1, AN300 and AC300 have acid site densities of 6.3 and 3.5 sites/m^2, respectively which is in fact higher than that of AN550 and AC550 i.e. 3.8 and 2.5 sites/m^2, respectively. From XRD (Fig. 1), AN300 has a mixture of (η-Al_2O_3 and gibbsite) phases while AC300 has only boehmite phase. On the other hand AN550 and AC550 have the η-Al_2O_3 and γ-Al_2O_3 phase, respectively. This means that different Al_2O_3 phase can be formed when starting with different precursors. Such significant differences in activity between AN catalysts and AC catalysts, may be attributed to the structure γ-Al_2O_3 which possessed almost hexagonally formed crystallites with an exposed surface of (1 1 0) planes preferentially whereas η-Al_2O_3 possessed relatively large particles, and the preferentially exposed surfaces correspond to the (1 1 1) crystallographic planes [27].

Furthermore given the relative difference in activities between the two precursors and their relative similarity in terms of surface area etc., for example, AN550 has higher DME formation rate than AC550 catalyst for all temperature ranges as shown in Fig. 8A and higher DME yield (see Table 1), this suggests that some poisoning of catalyst sites due to residual chloride may be responsible.

Fig. 8A shows the effect of reaction temperature on the DME formation rate (calculated based on Eq. (7)) over the produced AN550, AC550, a commercial γ-Al_2O_3 and a commercial HZSM-5(80). The most suitable dehydration catalysts should have a sufficient activity to generate the desired product but also prevent the production of by-products through further DME dehydration. In this case the selectivity to DME was almost 100% for all catalysts under the conditions used here. It can be seen that at low temperatures ranging from 180 °C to 275 °C, that the HZSM-5(80) has a higher reaction rate but as the temperature is increased to 275 °C the activity of AN550 catalyst increased is now higher than that of the HZSM-5 (80). From Fig. 7, the conversion of AC550 at 250 °C is 35.2% and from Fig. 8 the conversion of γ-Al_2O_3 is around 37%. This confirms that AC550 and γ-Al_2O_3 has the same structure.

Fig. 8B shows the methanol conversion as a function of time on stream over different acid catalysts at 250 °C. As before it is clear that the activity of catalyst increases in the following sequence: H-ZSM-5(80) > AN550 > AN650 > γ-Al_2O_3. All catalysts were stable over the reaction time. The methanol conversion over HZSM-5(80) zeolite decreased slightly from 85% to 82%, while AN550 decreased from 77% to 71.3% and for γ-Al_2O_3 decreased from 41% to 35% during a dehydration period of 70 h. This is likely attributed to coke formation over HZSM-5(80) [41] and to water adsorption on γ-Al_2O_3 and AN550. The result for HZSM-5(80) echoed an earlier

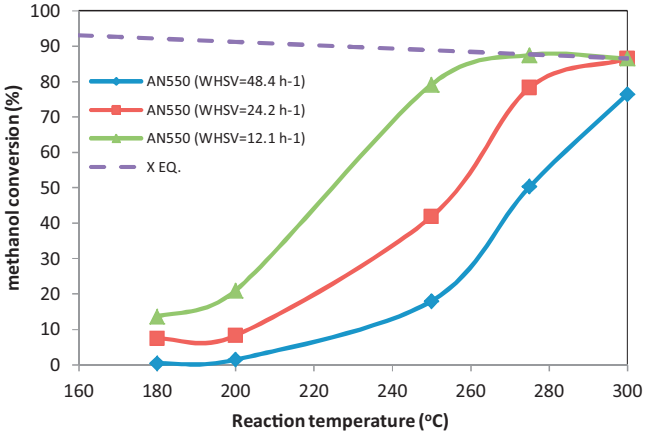

Fig. 9. Effect of space velocity of AN550 on methanol conversion to DME at different reaction temperature. He flow rate = 80 ml/min.

finding by Abu-Dahrieh et al. [41], which showed that coke formation over HZSM-5(80) is responsible for this deactivation. Although initially AN650 has a similar activity to AN550 it is less stable, as seen in the methanol conversion which decreased from 80% to 52%. This may be attributed to the appearance of although this could not be confirmed by the XRD (not shown) used herein [27]. From this it can seen that the activity of AN550 is two times the activity of commercial γ-Al_2O_3 and around 87% of HZSM-5(80) activity.

Fig. 9 shows the effect of space velocity on the activity of AN550. From the experimental data AN550 is active enough to give the equilibrium conversion of methanol at the reaction temperatures above 260 °C. From this it can be seen that an increase in catalyst mass leads to an increase in reaction rate where it can be observed that a linear relationship between catalyst mass and DME yield is obtained. Further increases in catalyst mass would therefore allow for higher conversions although this would introduce additional complications such as pressure drop.

4. Conclusions

Herein different acid catalysts were prepared using two precursors with different calcination temperatures during the production of DME from methanol. From the X-ray diffraction (XRD) pattern, different transition states of alumina were detected based on this calcination temperature. The boehmite was changed to γ-Al_2O_3 at 550 °C, and the bayerite was completely changed to η-Al_2O_3 when calcined at 550 °C. Among these catalysts that produced using the alumina nitrate precursor and calcined at 550 °C i.e. AN550 showed the highest catalytic performance under the reaction conditions (T = 180–300 °C, WHSV = 12.1 h^{-1}), compared it with AC550 and commercial γ-Al_2O_3 and higher than commercial zeolite HZSM-5 (80) for temperatures above 275 °C. A comparison showed that this material had double the activity of the (commercial γ-Al_2O_3 and AC550) and 87% activity of commercial HZSM-5(80) at 250 °C. The acid site density over catalysts changed with the calcination temperature. In the methanol dehydration, the acid site density affected catalytic performance among the catalysts with alumina phase structure. It is thus recommended that AN550 (η-Al_2O_3) is the most suitable catalyst for using in the production of DME from methanol.

References

[1] C. Paddock, Medical News Today (2012).
[2] F. Yaripour, F. Baghaei, I. Schmidt, J. Perregaard, Catalysis Communications 6 (2005) 147–152.
[3] Z. Zhu, D.K. Li, J. Liu, Y.J. Wei, S.H. Liu, Applied Thermal Engineering 35 (2012) 9–14.
[4] R. Ladera, E. Finocchio, S. Rojas, J.L.G. Fierro, M. Ojeda, Catalysis Today (2012).
[5] Q. Tang, H. Xu, Y. Zheng, J. Wang, H. Li, J. Zhang, Applied Catalysis A: General. 413–414 (2012) 36–42.
[6] A.R. Keshavarz, M. Rezaei, F. Yaripour, Journal of Natural Gas Chemistry 20 (2011) 334–338.
[7] F. Raoof, M. Taghizadeh, A. Eliassi, F. Yaripour, Fuel 87 (2008) 2967–2971.
[8] J. Khom-in, P. Praserthdam, J. Panpranot, O. Mekasuwandumrong, Catalysis Communications 9 (2008) 1955–1958.
[9] M. Mollavali, F. Yaripour, S. Mohammadi-Jam, H. Atashi, Fuel Processing Technology 90 (2009) 1093–1098.
[10] D. Liu, C. Yao, J. Zhang, D. Fang, D. Chen, Fuel 90 (2011) 1738–1742.
[11] S. Jiang, J.-S. Hwang, T. Jin, T. Cai, W. Cho, Y.s. Baek, S.-E. Park, Bulletin of the Korean Chemical Society 25 (2004) 185–189.
[12] M.R. Sun Kou, S. Mendioroz, P. Salerno, V. Munoz, Applied Catalysis A: General 240 (2003) 273–285.
[13] K. Lertjiamratn, P. Praserthdam, M. Arai, J. Panpranot, Applied Catalysis A: General 378 (2010) 119–123.
[14] F. Yaripour, F. Baghaei, I. Schmidt, J. Perregaard, Catalysis Communications 6 (2005) 542–549.
[15] J. Fei, Z. Hou, B. Zhu, H. Lou, X. Zheng, Applied Catalysis A: General 304 (2006) 49–54.
[16] Y. Fu, T. Hong, J. Chen, A. Auroux, J. Shen, Thermochimica Acta 434 (2005) 22–26.
[17] N. Khandan, M. Kazemeini, M. Aghaziarati, Applied Catalysis A: General 349 (2008) 6–12.
[18] F.S. Ramos, A.M.D.d. Farias, L.E.P. Borges, J.L. Monteiro, M.A. Fraga, E.F. Sousa-Aguiar, L.G. Appel, Catalysis Today 101 (2005) 39–44.
[19] M. Xu, J.H. Lunsford, D.W. Goodman, A. Bhattacharyya, Applied Catalysis A: General 149 (1997) 289–301.
[20] K.C. Tokay, T. Dogu, G. Dogu, Chemical Engineering Journal 184 (2012) 278–285.
[21] G.R. Moradi, F. Yaripour, P. Vale-Sheyda, Fuel Processing Technology 91 (2009) 461–468.
[22] V. Vishwanathan, K.-W. Jun, J.-W. Kim, H.-S. Roh, Applied Catalysis A: General 276 (2004) 251–255.
[23] M.S. Ghamsari, Z.A.S. Mahzar, S. Radiman, A.M.A. Hamid, S.R. Khalilabad, Materials Letters 72 (2012) 32–35.
[24] G.-f. Fu, J. Wang, J. Kang, Transactions of Nonferrous Metals Society of China 18 (2008) 743–748.
[25] Y.G. Wang, C. Suryanarayana, L.A. An, Journal of the American Ceramic Society 88 (2005) 780–783.
[26] L. Liu, W. Huang, Z.-h. Gao, L.-h. Yin, Journal of Industrial and Engineering Chemistry 18 (2012) 123–127.
[27] C.W. Seo, K.D. Jung, K.Y. Lee, K.S. Yoo, Industrial & Engineering Chemistry Research 47 (2008) 6573–6578.
[28] H. Knozinger, P. Ratnasamy, Catalysis Reviews-Science and Engineering 17 (1978) 31–70.
[29] V. Vatanpour, S.S. Madaeni, L. Rajabi, S. Zinadini, A.A. Derakhshan, Journal of Membrane Science 401–402 (2012) 132–143.
[30] Q. Yang, Bulletin of Materials Science 34 (2011) 239–244.
[31] S.A. Halawy, Chemical Monthly 134 (2003) 371–380.
[32] G.A.H. Mekhemer, S.A. Halawy, M.A. Mohamed, M.I. Zaki, Journal of Physical Chemistry B 108 (2004) 13379–13386.
[33] W.Q. Jiao, M.B. Yue, Y.M. Wang, M.-Y. He, Microporous and Mesoporous Materials 147 (2012) 167–177.
[34] K. Wefers, C. Misra, Alcoa Technical Paper No. 19, Revised, 1987.
[35] P.S. Santos, H.S. Santos, S.P. Toledo, Materials Research 3 (2000) 104–114.
[36] A.L. Dragoo, J.J. Diamond, Journal of the American Ceramic Society 50 (1967) 568–574.
[37] K. Sohlberg, S.T. Pantelides, S.J. Pennycook, Journal of the American Chemical Society 123 (2001) 26–29.
[38] H.S. Potdar, K.-W. Jun, J.W. Bae, S.-M. Kim, Y.-J. Lee, Applied Catalysis A: General 321 (2007) 109–116.
[39] J. Aguado, J.M. Escola, M.C. Castro, B. Paredes, Applied Catalysis A: General 284 (2005) 47–57.
[40] B. Chakraborty, B. Viswanathan, Catalysis Today 49 (1999) 253–260.
[41] J. Abu-Dahrieh, D. Rooney, A. Goguet, Y. Saih, Chemical Engineering Journal 203 (2012) 201–211.